Originally submitted to *Nature*, July 15, 2003.

Revised, November 24, 2003.

Cooling history of the Pacific lithosphere

Michael H. Ritzwoller, Nikolai M. Shapiro, & Shi-Jie Zhong

Department of Physics, University of Colorado at Boulder, Boulder, CO 80309-0390 USA

Plate tectonics is expressed most simply in oceanic plates where a thermal boundary layer or "lithosphere" forms as the plate cools during its journey away from mid-ocean ridges[1-2]. Based on a seismic model of the Pacific upper mantle inferred from a new compilation of seismic surface wave dispersion measurements, we show that, on average, the Pacific lithosphere has experienced a punctuated cooling history, cooling diffusively for its first 70 Ma and then reheating in the Central Pacific between ages of 70 and 100 Ma predominantly at depths between 70 and 150 km. From 100 Ma to about 135 Ma, the processes of reheating are substantially weaker than in the Central Pacific. The cause of the reheating in the Central Pacific remains unclear. We show, however, that thermal boundary layer instabilities (TBI) form naturally as the plate cools and, with the right rheology, may help to explain the mean characteristics of the observed cooling history of the Pacific plate.

Few observables directly constrain the thermal state of the oceanic lithosphere or the "asthenosphere" that lies beneath it. Seafloor topography and heat flow[3-5] have been most commonly used to infer oceanic mantle temperatures as these surface observables reflect the average temperature and the temperature gradient in the uppermost mantle. The lithosphere is believed to cool with age because of the deepening of the sea-floor and the reduction in heat flow away from the mid-ocean ridges, but these trends cease and topography becomes much more erratic by about 80 Ma. Seismic waves provide a more direct probe of mantle structures, and seismic models have recently revealed that the Central Pacific hosts several intriguing features, including anomalous asthenospheric radial anisotropy[6], changes in the strength and orientation of azimuthal anisotropy[7,8], and the existence of upper mantle and transition zone anelastic anomalies[9]. The application of seismic models to sub-oceanic lithospheric geothermometry, however, has been limited due to substantial uncertainties in the conversion from seismic velocities to temperatures and by poor station coverage across the Pacific seafloor which has reduced both lateral and, more significantly, vertical resolution. Both issues have been increasingly ameliorated in recent years due to the growth of the global seismic network and advances in the theory of thermoelasticity[10].

Surface waves provide the most uniform coverage of the Pacific lithosphere of all seismic waves

and now densely sample most of the Pacific basin (see supplementary information). Figure 1a-c shows several surface wave speed maps across the Pacific[11], referenced to the prediction for a diffusively cooling half-space (Half-Space Cooling or HSC model[2]). For lithospheric ages younger than about 70 Ma, there is good agreement on average between the observed surface wave speeds and those predicted from the HSC model. A systematic deviation from the surface wave speeds predicted from the HSC model appears in the Central Pacific at a lithospheric age of about 70 Ma. In particular, wave speeds are depressed relative to the HSC model prediction in a north-south band across the Central Pacific ranging from about 70 to 100 Ma and, on average, remain lower than the speeds predicted by the HSC model in the Western Pacific. The details of this discrepancy depend on wave type and period. The observation of the discrepancy is robust to data subsetting, to changes in the the theory of wavefield sensitivity (ray versus diffraction tomography[11]), and to the simultaneous inversion for azimuthal anisotropy, but requires a lateral resolution of better than 1200 km (where resolution is defined as twice the standard deviation of the Gaussian fit to the resolution surface).

These observations of surface wave dispersion strongly constrain shear velocities which are related to temperatures in the uppermost mantle[10]. Using surface wave dispersion maps across the Pacific we estimated a radially anisotropic (transverse isotropy with a radial symmetry axis) three dimensional (3-D) tomographic model of shear-wave speed in the Earth's upper mantle by a Monte-Carlo method[12] using both seismic and temperature parameterizations. Inferences are similar from both parameterizations (see supplementary information), but we present results only from the temperature parameterization, which is based on a thermal model of the oceanic lithosphere and asthenosphere[13] with two principal mantle unknowns. The first unknown is the "apparent thermal age" of the lithosphere and the second unknown is the "potential temperature" of the asthenosphere which is the upward continuation to the surface of asthenospheric temperatures following the mantle adiabatic gradient. The results of the inversion at a point in the Central Pacific are shown in Figure 2.

Figures 3a and 3b present the 3-D shear-velocity model at a depth of 100 km in the uppermost mantle. The general increase in shear-wave speed toward the western Pacific, as seen in Figure 3a, is consistent with the prediction from the HSC model. As Figure 3c shows, until about 70 Ma the age trend of the shear velocities at 100 km depth are, on average, in remarkable agreement with the predictions from the HSC model. Reflecting the information in the wave speed maps, a systematic deviation from the HSC model develops in the Central Pacific at lithospheric ages that range from about 70 Ma to somewhat more than 100 Ma (Fig. 3b-c). This deviation appears as a low shear-wave velocity anomaly running generally north-south in a crescent shaped feature across

the Central Pacific, largely confined in the era between the 70 Ma and 105 Ma age contours in Figure 3b. The reduction of shear-wave speed in this era is a persistent feature of the inversion. Above and below 100 km depth, the pattern of the deviation is similar but the amplitude decreases (Fig. 3d-e). As seen in Figure 3f, the average Pacific isotachs deepen with lithospheric age, following the HSC model until about 70 Ma and then flatten until about 105 Ma, after which they deepen again. This deviation is shown in Figure 3g to set-on abruptly at about 70 Ma and maximizes in the deep lithosphere and shallow asthenosphere at depths between 70 km and 150 km. The approximately uniform deviation deeper than 100 km is caused by the fact that the HSC reference model does not include adiabatic heating with depth.

The same trend with lithospheric age is revealed in the temperature structure seen in Figure 4. Lithospheric temperatures are summarized by the observed apparent thermal age, shown in Figure 4b. The apparent thermal age diverges systematically from the lithospheric age at about 70 Ma and remains depressed throughout most of the old Pacific (Fig. 4c,e). The deficit in apparent lithospheric age that develops in the Central Pacific, referred to elsewhere as thermal resetting or extent of rejuvenation[5], is seen in Figure 4d to grow until it reaches more than 30 million years at a lithospheric age of 100 Ma. After this age, the age deficit is approximately constant, on average, but becomes highly variable in the very old Pacific at lithospheric ages greater than about 135 Ma. In terms of temperatures, average Pacific isotherms deepen with lithospheric age, as Figure 4e shows, agreeing with the HSC model until about 70 Ma where they flatten until about 100 Ma and deepen again until about 135 Ma. By 100 Ma, average temperatures in the Pacific lithosphere at 100 km depth deviate from the temperatures of the HSC model by more than 100°C.

Our results demonstrate that the seismic and thermal structures of the Pacific lithosphere deviate systematically from a model whose heat flux is dominated by diffusive cooling alone. Although temperatures of formation may have been higher between 70 Ma and 100 Ma than they were prior or subsequent to this era[14], the temperature anomalies observed in Figure 4e are probably too large to be the residual of elevated temperatures of formation and we do not find elevated average temperatures during this era in other oceans (see supplementary information). For these reasons, we conclude that the processes that have reheated the lithosphere are likely to be on-going. The age trend of lithospheric structure, therefore, suggests two phases of Pacific lithospheric cooling, from 0 Ma to 70 Ma and another from 100 Ma to ∼135 Ma, bracketing an era of lithospheric reheating during which an average thermal resetting of more than 30 Ma develops. At ages older than 135 Ma, the thermal state of the lithosphere is highly variable and the statistics of inference are less favorable as the area covered by old lithosphere is small.

The reheating of the Pacific upper mantle has been proposed previously based largely on surface

observables, such as seafloor topography and heat flow evidence[5]. Various convective processes have been hypothesized as the cause of lithospheric reheating, including those confined to the upper mantle (e.g., small-scale convection directly beneath the lithosphere[15–17] or larger scale convection across the entire upper mantle[18]) and those that extend considerably deeper into the lower mantle (e.g. hot spot plumes[19,20] or larger scale limbs of global convection possibly associated with superswells[21]). Near-surface structures, such as the accumulation of sediments, the formation of volcanic edifices, and associated crustal thickening, however, obscure the interpretation of surface observables alone, and our results provide the first direct evidence of the time-history (70 - 100 Ma) and depth extent (70 - 150 km) of reheating.

Recent seismic evidence points to a superplume that may heat the Central Pacific[6,9], but the mechanics of heat transport from the upper mantle into the high viscosity lithosphere remain unclear. One possible mechanism is the development of thermal boundary layer instabilities (TBI), or small-scale convection, that remove the deep lithosphere and replace it with relatively hot asthenospheric material. The development of TBI may, indeed, be triggered and modulated by upwelling thermal plumes[22], but TBI also develops spontaneously without the influence of plumes as the lithosphere cools and thickens with age[15–17]. Although the potential role of a thermal plume in the dynamics of TBI has been studied for the Hawaiian swell[22], superplumes at the Pacific plate scale are not well understood dynamically. For this reason, in order to examine the effects of TBI on lithospheric thermal structure we have simulated TBI without imposing thermal plumes. Convection cells formed as a result of TBI are too small to be imaged directly by our seismic model. Aspects of the larger-scale thermal anomalies apparent in the seismic model, however, may be caused by TBI. We discuss here only whether the consequences of TBI can match the average cooling history of the Pacific lithosphere, in particular lithospheric reheating that occurs in a discrete time interval from 70 to 100 Ma. We do not attempt to model or explain the considerable isochronous variability of the observed seismic and temperature structures.

Using a 3-D mantle convection model with temperature-dependent viscosity, the simulated TBI initiates when the lithosphere is $\sim$70 Ma old, forms convective rolls oriented approximately along the direction of plate motion with characteristic diameters between 100 - 200 km[23], reheats the lithosphere to temperatures higher than in the HSC model[17,24], and cools the asthenosphere. The onset time of TBI is controlled mainly by asthenospheric viscosity and activation energy[17,24,25], but the temperature anomalies caused by TBI, which determine the extent of lithospheric reheating and its time evolution, depend dominantly on rheological activation energy[17,24]. Analogous to the seismic results, we quantify the extent of lithospheric reheating by estimating the apparent thermal age of the lithosphere by fitting an error function (eqn. 1) to the simulated temperature structure.

We find that, with a judicious choice of rheology, TBI can reheat the lithosphere to match the average cooling history of the Pacific lithosphere (Fig. 4d and supplementary information). As shown in Figure 4d, after the onset of TBI, the apparent thermal age remains approximately constant for a period of ~25 Ma after which the apparent thermal age increases again. Although TBI remains active after 100 Ma, it is less vigorous because increases in asthenospheric viscosity caused by TBI at younger ages reduce asthenospheric temperatures[23]. A good match between the simulated and observed cooling histories is achieved with an effective rheological activation energy of 120 kJ/mol, similar to the value inferred from flexural deformation near seamounts[26].

Although TBI can explain the average cooling history of the Pacific lithosphere, our simulations do not explain the variation within lithospheric age ranges observed seismically. To explain this variability may require additional physical processes not included in the simulations presented here, such as variations in the conditions of formation of the lithosphere, the effects of thermal plumes, or non-Newtonian rheology. Plumes, in particular, are likely to play an important, but geographically variable, role in the onset and stabilization of TBI.

Methods

Construction of the 3-D shear velocity and temperature models

The inversion for a radially anisotropic 3-D tomographic model of shear-wave velocity and temperature is performed in two steps. In the first step, we compiled a large new data set of broad-band group velocity measurements and produced Rayleigh and Love wave group velocity maps[11] on a $2^\circ \times 2^\circ$ grid across the Pacific from 18 sec period to 200 sec for Rayleigh waves and from 20 sec to 150 sec for Love waves. There are more than 200,000 measurement paths world-wide. We also constructed phase velocity maps using measurements compiled at Harvard[6] and Utrecht[27] Universities from 40 sec to 150 sec period. The great length of most wavepaths across the Pacific necessitates considering the path-length dependent spatial sensitivity of the surface waves in order to model wave-front healing and associated diffraction effects[11]. The joint inversion of group and phase velocities gives better vertical resolution than either data type alone (see supplementary information), providing unique information about the vertical variability of shear velocities in the uppermost mantle.

In the second step, the dispersion maps are used to construct a 3-D model on a $2^\circ \times 2^\circ$ grid to 400 km depth based on two separate parameterizations: a seismic parameterization[12] and a temperature parameterization derived from a thermal model[13]. The seismic parameterization consists of 13 unknowns, seven in the crust and six in the mantle. The crust consists of three layers in which compressional (V_p) and shear (V_s) velocity are free variables as is crustal thickness; all seven crustal unknowns are perturbed from reference values taken from the model CRUST2.0 (G. Laske, personal communication, 2002). Isotropic mantle structure is parameterized with four radial cubic B-splines. The remaining two unknowns parameterize radial anisotropy. Because Rayleigh waves are predominantly sensitive to V_{sv} and Love waves to V_{sh}, we have constraints on only two of the five elastic moduli that describe a transversely isotropic medium. The basis functions for radial anisotropy represent the bifurcation of V_{sh} and V_{sv} in the uppermost mantle to a depth of 220 km and are sufficiently flexible to accommodate the unusual anisotropy in the Central Pacific[6]. The effective isotropic shear velocity, V_s, is defined as the average of the anisotropic velocities.

The inversion proceeds by Monte-Carlo sampling that walks randomly through a subspace of model space defined by a-priori constraints and forms a Markov-chain similar to Brownian motion. At each point on the $2^\circ \times 2^\circ$ grid, an ensemble of acceptable vertical profiles emerges (e.g., Fig. 2c,d). The Monte-Carlo inversion estimates a range of seismic and temperature models at each depth so that only features that appear in every member of the ensemble of acceptable models are interpreted. We refer to these features as "persistent". When a single model is needed, we use the middle of the ensemble of acceptable models.

The temperature parameterization (Fig. 2b) is based on a thermal model in which a thermally conductive layer (lithosphere) overlies a convective layer (asthenosphere) joined smoothly by a transition layer. The temperature profile within the conductive layer is described by the half-space cooling solution,

$$T(z) = T_s + (T_m - T_s)\ \mathrm{erf}\left(z/2\sqrt{\kappa\tau}\right), \tag{1}$$

where z is depth in the mantle, T_m is initial mantle temperature fixed at 1300°C, $T_s = 0$°C is the surface temperature, thermal diffusivity $\kappa = 1 \times 10^{-6}$ m^{2}s^{-1}, and τ is the "apparent thermal age" of the lithosphere. In the convective layer, the adiabatic temperature gradient $D_a = 0.5$°C/km and the potential temperature T_p describe the thermal state of the asthenosphere.

Two mantle unknowns in the temperature parameterization specify the thermal state of the oceanic upper mantle: τ in the lithosphere and T_p in the underlying asthenosphere. These two unknowns replace the four B-splines in the seismic parameterization. The Monte-Carlo inversion with the temperature parameterization initiates in temperature space where a trial thermal model is constructed and is converted to shear velocity in the mantle, then trial seismic crustal structures are introduced as well as mantle radial anisotropy similar to the generation of these features in the seismic parameterization. The temperature profiles that fit the seismic data acceptably for an appropriate subset of seismic crustal models and models of radial anisotropy define the ensemble of acceptable profiles in temperature space and are also combined with the crustal and radial anisotropic models to define the ensemble of acceptable models in seismic velocity space.

Interconversion between temperature and shear velocity

Interconversion between temperature and shear velocity is based on laboratory-measured thermoelastic properties of mantle minerals represented as partial derivatives of the elastic moduli with respect to temperature, pressure, and composition[10]. The compositional model for the oceanic upper mantle includes 75% Olivine, 21% Orthopyroxene, 3.5% Clinopyroxene, and 0.5% Spinel with an Iron-to-Magnesium ratio of 10%[28]. We compute shear velocity with the anelastic correction[10] from an anharmonic shear velocity, $v_{anel}(P,T,\omega) = v(P,T)\left[1 - \left(2Q_\mu^{-1}(P,T,\omega)/\tan(\pi a/2)\right)\right]$, using a temperature dependent Q-model, $Q_\mu(P,T,\omega) = A\omega^a \exp\left[a(H^* + PV^*)/RT\right]$, where R is the gas constant and we set the exponent $a = 0.15$, anelastic activation energy $H^* = 500$ kJ/mol, anelastic activation volume $V^* = 2.0 \times 10^{-5}$ m^3/mol, and the amplitude $A = 0.049$.

Half-Space Cooling (HSC) Model

The vertical temperature profile of the HSC model[2] is the solution to the one dimensional thermal diffusion equation for an infinite half-space, which takes the same form as equation (1). In contrast

with the temperature parameterization for the seismic inversion, the error-function temperature profile for the HSC model continues infinitely with depth and explicitly does not include adiabatic heating. Predictions from the HSC model are intended to represent age trends expected for purely diffusive cooling. Several ad-hoc choices (e.g., T_m, the Q-model) in specifying the HSC model create uncertainty in the absolute level of temperatures and seismic velocities in the mantle. We account for this in Figures 1 and 3c-e, by shifting the HSC predictions to fit the observations optimally between 10 Ma and 60 Ma. This shift also approximately corrects for the effect of adiabatic heating.

Simulating Thermal Boundary Layer Instabilities

Our 3-D Cartesian convection model uses a depth- and temperature-dependent Arrhenius rheology with flow-through boundary conditions[23]. The model box is 1000 km deep, 12,000 km long (in the direction of plate motion), and 3,000 km wide. At the surface, temperature is 0°C and plate velocity is 5 cm/year, while at the bottom of the box temperature is 1350° C and velocity is zero. The inflow boundary has temperatures corresponding to 10 Ma old lithosphere with velocities derived from a Couette flow. The outflow boundary has zero vertical temperature gradient and the same velocities as the inflow. The other two sidewalls (i.e., parallel to plate motion) have reflecting boundary conditions. The viscosity law is $\eta(z,T) = \eta_0(z)\exp(E/RT)$ where the pre-factor $\eta_0(z)$ is constant above 400 km depth and increases by a factor of 19 and 190 in the transition zone and lower mantle, respectively, compared with that in the upper mantle[24]. The viscosity in the upper mantle is about 4×10^{19} Pa-s and rheological activation energy is 120 KJ/mol. This leads to ~70 Ma onset time for TBI[24]. This activation energy is consistent with that inferred from the study of flexural deformation near seamounts[26]. Because we employ a Newtonian rheology, however, the activation energy may be viewed only as an "effective" rheological parameter for the mantle with a non-Newtonian rheology[29]. The models are computed to a statistical steady-state. Other model parameters are thermal diffusivity of 10^{-6} m^2/s, coefficient of thermal expansion of 3×10^{-5} K^{-1}, mantle density of 3,300 kg/m^3, and gravitational acceleration equal to 9.8 m/s^2.

References

1. McKenzie, D.P., Some remarks on heat flow and gravity anomalies, *J. Geophys. Res., 72*, 6261-6273, 1967.

2. Parker, R.L. & Oldenburg, D.W., Thermal model of ocean ridges, *Nature Phys. Sci., 242*, 137-139, 1973.

3. Parsons, B. & Sclater, J.G., An analysis of the variation of ocean floor bathymetry and heat flow with age, *J. Geophys. Res., 82*, 803-827, 1977.

4. Stein, C. A. & Stein, S., A model for the global variation in oceanic depth and heat flow with lithospheric age, *Nature, 359*, 123-129, 1992.

5. Nagihara, S., Lister, C.R.B., & J.G. Sclater, Reheating of old oceanic lithosphere: Deductions from observations, *Earth Planet. Sci. Letts., 139*, 91-104, 1996.

6. Ekström, G. & Dziewonski, A.M., The unique anisotropy of the Pacific upper mantle, *Nature*, *394*, 168-172, 1998.

7. Ekström, G., Mapping the lithosphere and asthenosphere with surface waves: Lateral structure and anisotropy, in *The History and Dynamics of Global Plate Motions*, ed. M.A. Richards, R.G. Gordon, R.D. van der Hilst, Amer. Geophys. Un. Geophys. Monogr. 121, 239-256, Washington, D.C., 2000.

8. Trampert, J. & Woodhouse, J.H., Global anisotropic phase velocity maps for fundamental mode surface waves between 40 s and 150 s, *Geophys. J. Int., 154*, 154-165, 2003.

9. Romanowicz, B. & Gung, Y., Superplumes from the core-mantle boundary to the lithosphere: Implications for heat flux, *Science, 296*, 513-516, 2002.

10. Goes, S., Govers, R., & Vacher, R., Shallow mantle temperatures under Europe from P and S wave tomography, *J. Geophys. Res., 105*, 11,153-11,169, 2000.

11. Ritzwoller, M.H., Shapiro, N.M., Barmin, M.P., & Levshin, A.L., Global surface wave diffraction tomography, *J. Geophys. Res., 107(B12)*, 233, 2003.

12. Shapiro, N.M. & Ritzwoller, M.H., Monte-Carlo inversion for a global shear velocity model of the crust and upper mantle, *Geophys. J. Int., 51*, 88-105, 2002.

13. Shapiro, N.M. & Ritzwoller, M.H., Thermodynamic constraints on seismic inversions, *Geophys. J. Int.*, submitted, 2003.

14. Larson, R.L., Latest pulse of Earth: Evidence for a mid-Cretaceous superplume, *Geology, 19*, 547-550, 1991.

15. Richter, F. M. & Parsons, B., On the interaction of two scales of convection in the mantle, *J. Geophys. Res., 80*, 2529-2541, 1975.

16. Parsons, B. & McKenzie, D., Mantle convection and thermal structure of the plates, *J. Geophys. Res., 83*, 4485-4496, 1978.

17. Davaille, A. & Jaupart, C., Onset of thermal convection in fluids with temperature-dependent viscosity: application to the oceanic lithosphere, *J. Geophys. Res., 99*, 19,853-19,866, 1994.

18. Houseman, G. & McKenzie, D.P., Numerical experiments on the onset of convective instability in the Earth's mantle, *Geophys. J. R. Astron. Soc., 68*, 133-164, 1982.

19. Crough, S.T., Thermal origin of mid-plate hot-spot swells, *Geophys. J. R. Astron. Soc., 55*, 451-470, 1978.

20. Schroeder, W., The empirical age-depth relation and depth anomalies in the Pacific Ocean, *J. Geophys. Res., 89*, 9873-9884, 1984.

21. McNutt, M.K., Superswells, *Revs. Geophys., 36*, 211-244, 1998.

22. Moore, W.B., Schubert, G. & Tackley, P., Three-dimensional simulations of plume-lithosphere interaction at Hawaiian Swell, *Science, 279,* 1008-1011, 1998.

23. van Hunen, J., Huang, J., & Zhong, S., The effect of shearing on onset and vigor of small-scale convection with a Newtonian rheology, submitted to *Geophys. Res. Lett.*, 2003.

24. Huang, J., Zhong, S. & van Hunen, J. Controls on sub-lithospheric small-scale convection, *J. Geophys. Res.*, in press, 2003.

25. Korenaga, J. & Jordan, T. H., Physics of multiscale convection in Earth's mantle: Onset of sublithospheric convection, *J. Geophys. Res., 108(B7)*, 2333, 2003.

26. Watts, A.B. & Zhong, S., Observations of flexure and the rheology of oceanic lithosphere, *Geophys. J. Int., 142*, 855-875, 2000.

27. Trampert, J. & Woodhouse, J.H., Global phase velocity maps of Love and Rayleigh waves between 40 and 150 s period, *Geophys. J. Int.122*, 675-690, 1995.

28. McDonough, W.F. & Rudnick, R.L., Mineralogy and composition of the upper mantle, in: *Ultrahigh-pressure mineralogy: physics and chemistry of the Earth's deep interior*, R.J. Hemley, Editor, 139-164, Mineralogical Society of America, Washington, DC, 1998.

29. Christensen, U. R., Convection with pressure and temperature dependent non-Newtonian rheology, *Geophys. J. R. Astron. Soc., 77*, 242 284, 1984.

30. Mueller, R.D., Roest, W.R., Royer, J.-Y., Gahagan, L.M., & Sclater, J.G., Digital isochrons of the world's ocean floor, *J. Geophys. Res., 102*, 3211-3214, 1997.

Acknowledgements. The authors gratefully acknowledge critical reviews from Jeannot Trampert and Geoff Davies. The data used in this work were obtained from the IRIS Data Management Center and the GEOSCOPE Data Center. The authors are grateful to researchers at Harvard and Utrecht Universities for contributing phase velocity measurements to this study. We thank Anatoli Levshin, William Landuyt, Rosa Bernal, Liz Zea, and Abir van Hunen for help in preparing the data set. Aspects of this work were supported by the US National Science Foundation and the Packard Foundation.

Supplementary information accompanies the paper at:

http://ciei.colorado.edu/pubs/2003/7_suppl.pdf

Competing interests statement. The authors declare that they have no competing financial interests.

Correspondence and requests for materials should be addressed to M.H.R.

(ritzwoller@ciei.colorado.edu)

This manuscript is available electronically at:

http://ciei.colorado.edu/pubs/2003/7.pdf

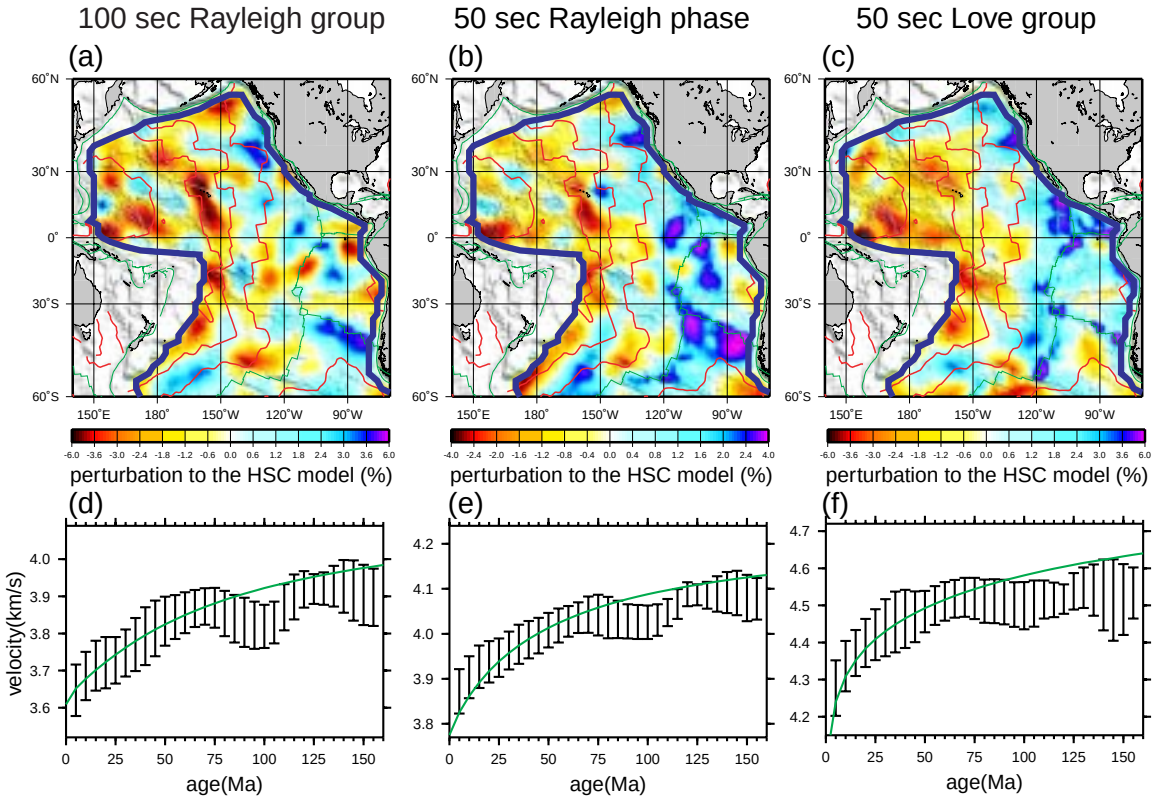

Figure 1: **Surface wave speed maps and trends with lithospheric age.** (a) - (c) Maps of surface wave speed plotted as a percent perturbation to the speed predicted from the HSC model (green lines in (d) - (f)) for 100 sec Rayleigh wave group speed, 50 sec Rayleigh wave phase speed, and 50 sec Love wave group speed, respectively. The green lines denote plate boundaries, the red lines are isochrons of lithospheric age in increments of 35 Ma, and the blue contour encloses the region where there are lithospheric age estimates[30]. (d) - (f) Surface wave speed, averaged in 5 Ma lithospheric age bins across the Pacific, is plotted versus lithospheric age for the maps in (a) - (c), respectively. "Error" bars represent the standard deviation within each age range. Predictions from the HSC model in (a) - (f) are shifted to fit the observations optimally between 10 Ma and 60 Ma: -70 m/s in (a) & (d), -80 m/s in (b) & (e), and 10 m/s in (c) & (f). This shift accommodates radial anisotropy and arbitrary choices in the definition of the HSC model (e.g., initial mantle temperature).

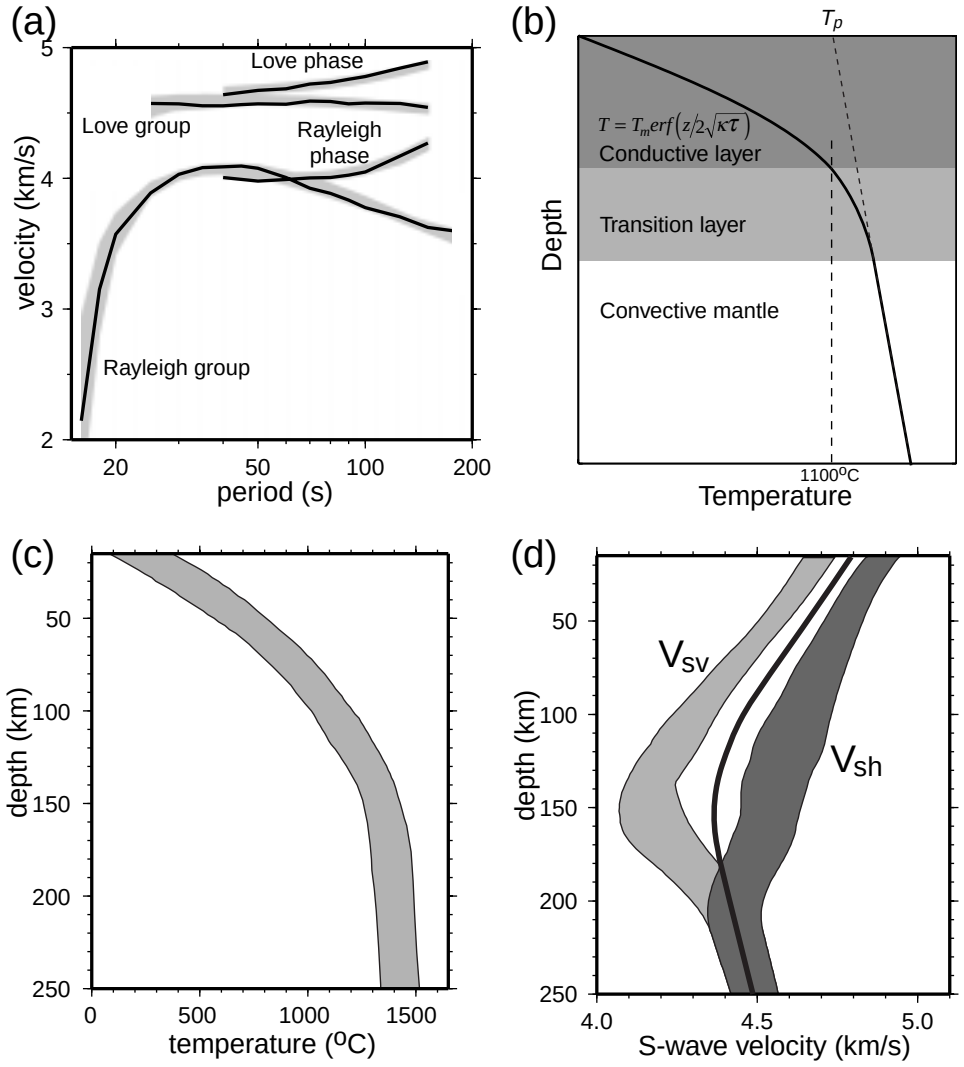

Figure 2: **Construction of the 3-D model at a point in the Central Pacific.** (a) The four observed dispersion curves at a location in the Central Pacific (14°N, 200°E) are plotted with black lines. (b) The temperature parameterization is based on a thermal model in which an error function, which represents temperatures in the lithosphere (eqn. 1), is underlain by an adiabatic gradient in the convective mantle (asthenosphere), joined smoothly by a transition region. The unknown in the conductive layer is the apparent thermal age, τ, and the unknown in the underlying asthenosphere is the potential temperature, T_p. (c) & (d) Inversion results for the Central Pacific location. The ensemble of acceptable temperature models in the uppermost mantle is shown in (c). The ensemble of seismic models is displayed in (d), where the light grey-shaded envelope is V_{sv} and the dark grey-shaded envelope is V_{sh}. The thick black line is the median of the ensemble of isotropic shear velocities, V_s. This example demonstrates the unusual anisotropy in the Central Pacific[6] in which the bifurcation between V_{sv} and V_{sh} grows with depth, maximizing here at about 140 km. Predictions from the ensemble of acceptable models to the four observed dispersion curves are shown as grey lines in (a).

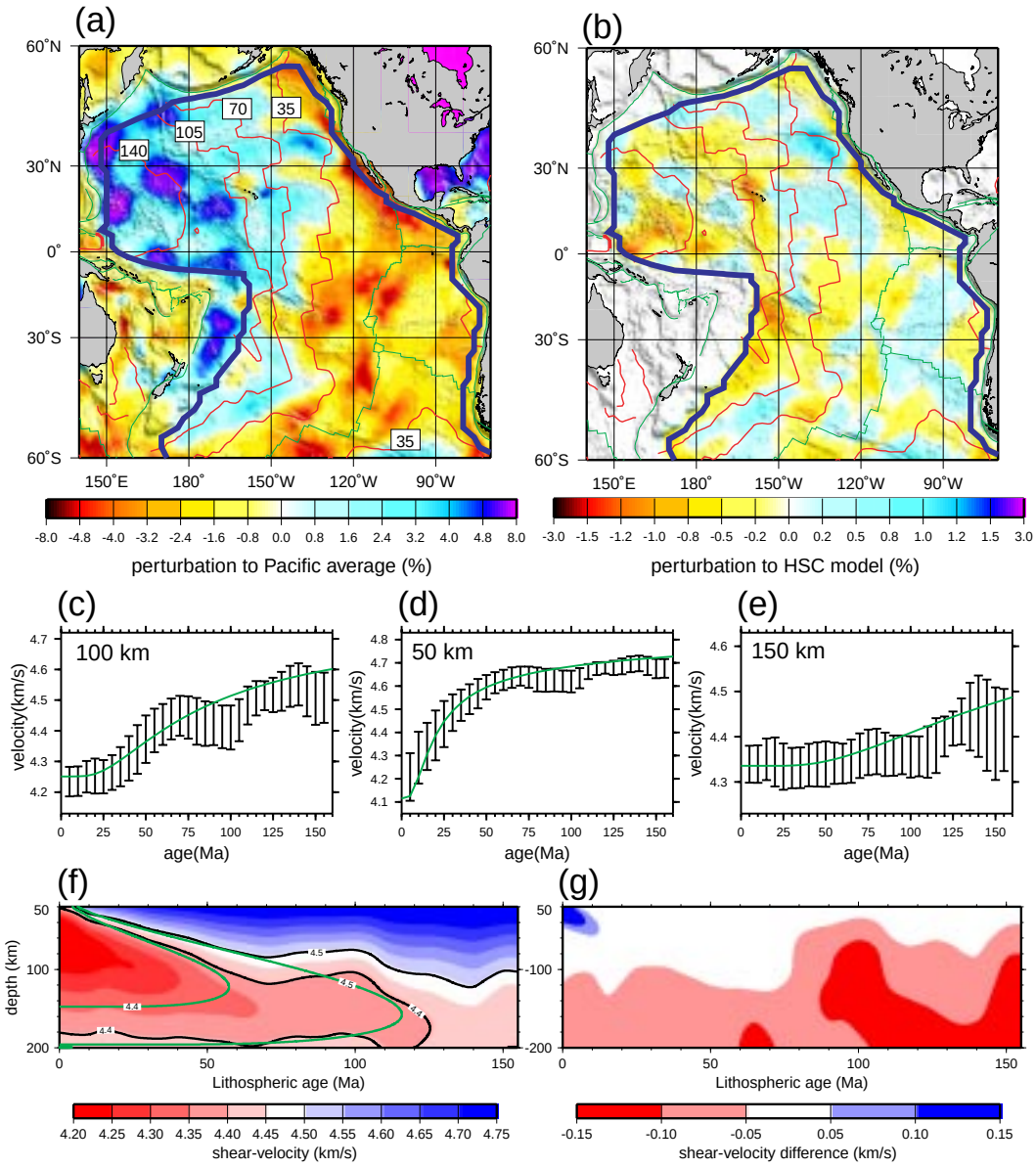

Figure 3: **Shear velocity structure of the Pacific upper mantle and trend with lithospheric age.** (a) Shear velocity at 100 km depth, presented as a perturbation to the average across the Pacific (4.362 km/sec). The green, red, and blue lines are as in Figure 1a-c. (b) Shear velocity at 100 km depth presented as a perturbation to the prediction from the HSC model. (c) - (e) Shear velocity, averaged in 5 Ma lithospheric age bins across the Pacific, is plotted versus lithospheric age at 100 km, 50 km, and 150 km depths. "Error" bars represent the standard deviation within each age range. The continuous green lines are the predictions from the HSC model shifted vertically to fit the observations optimally between 10 Ma and 60 Ma: -30 m/s at 100km, -10 m/s at 50 km, and -70 m/s at 150 km. (f) V_s averaged across the Pacific plotted versus lithospheric age. The green lines are isotachs (lines of constant shear velocity) from the HSC model. (g) Difference between the Pacific average shear velocity and the prediction from the HSC model. Reds identify areas where the observed shear velocity is slower than the HSC model predicts.

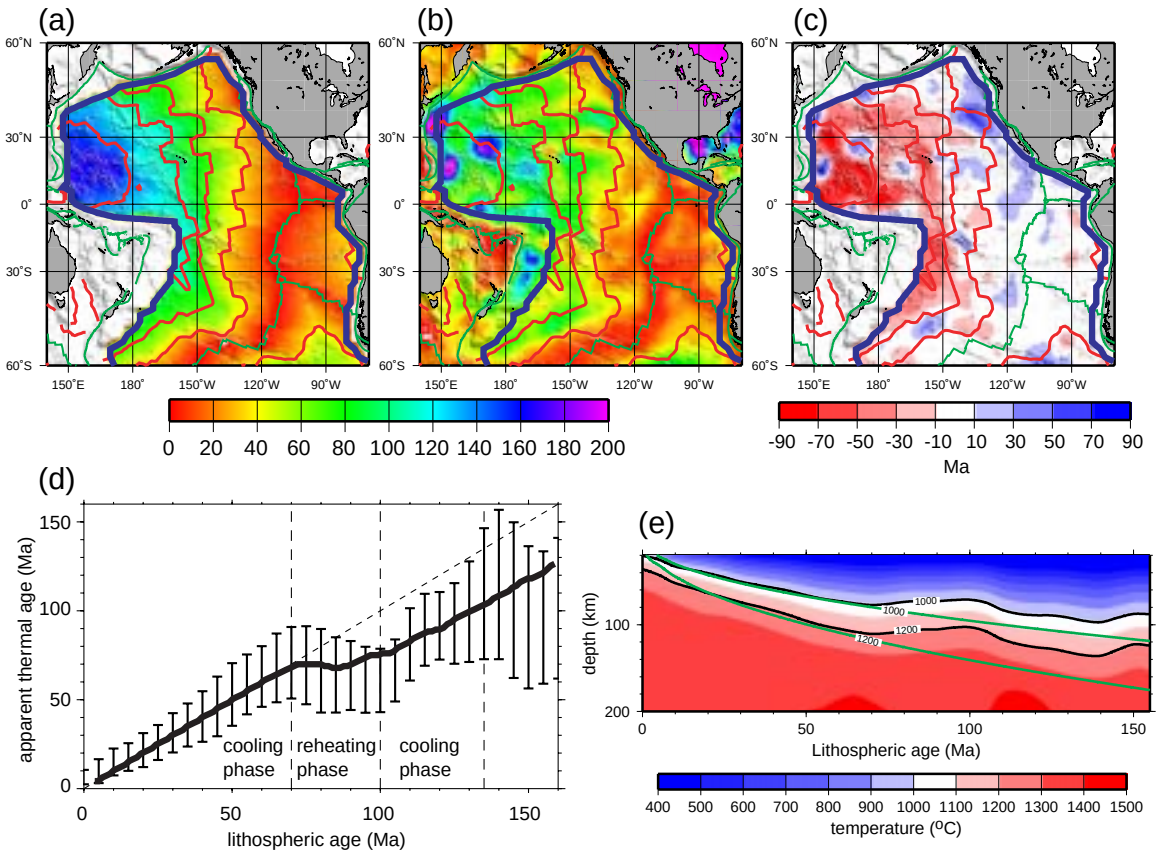

Figure 4: **Thermal structure of the Pacific upper mantle and trend with lithospheric age.** (a) Lithospheric age in Ma, presented as a reference[30]. (b) Estimated apparent thermal age, τ. (c) Difference between the lithospheric age and the apparent thermal age. Reds imply that the apparent thermal age is younger than the lithospheric age. In (a) - (c), the green, red, and blue lines are as in Figure 1a-c. (d) The "error" bars represent the standard deviation of τ within each 5 Ma lithospheric age bin averaged across the Pacific. Two lithospheric cooling phases are identified, 0 - 70 Ma and 100 - 135 Ma, bracketing a phase in which the Pacific lithosphere undergoes reheating. The thick black line is τ, similarly averaged in lithospheric age bins, computed from the 3-D convection model of thermal boundary layer instabilities, with an effective rheological activation energy of 120 kJ/mol. (e) Upper mantle temperature averaged across the Pacific plotted versus lithospheric age. The green lines are isotherms from the HSC model. An average perturbation of more than 100°C develops between the observed and HSC temperature profiles at a depth of about 100 km due to processes of reheating that occur between 70 and 100 Ma in the Central Pacific.